Supporting Information

Overcoming Residual Carbon-Induced Recombination in Water-Oxidation Catalysis: Combining a Superior Catalyst with Low-Carbon-Content Atomic Layer Deposition of SnO_2 for Improved Catalysis

Carly F. Jewell, [†], Ashwanth Subramanian, [#] Won-Il Lee, [#] Chang-Yong Nam, [*, ‡, #] Richard G. Finke[*, †]

[†]Department of Chemistry, Colorado State University, Fort Collins, Colorado, 80523, United States

[#]Department of Materials Science and Chemical Engineering, Stony Brook University, Stony Brook, New York, 11794, United States

[‡]Center for Functional Nanomaterials, Brookhaven National Laboratory, Upton, New York, New York 11973, United States

*Corresponding author emails: *Richard.Finke@colostate.edu; cynam@bnl.gov

Table of Contents

S1. XPS of Li-IrO_x

(a)

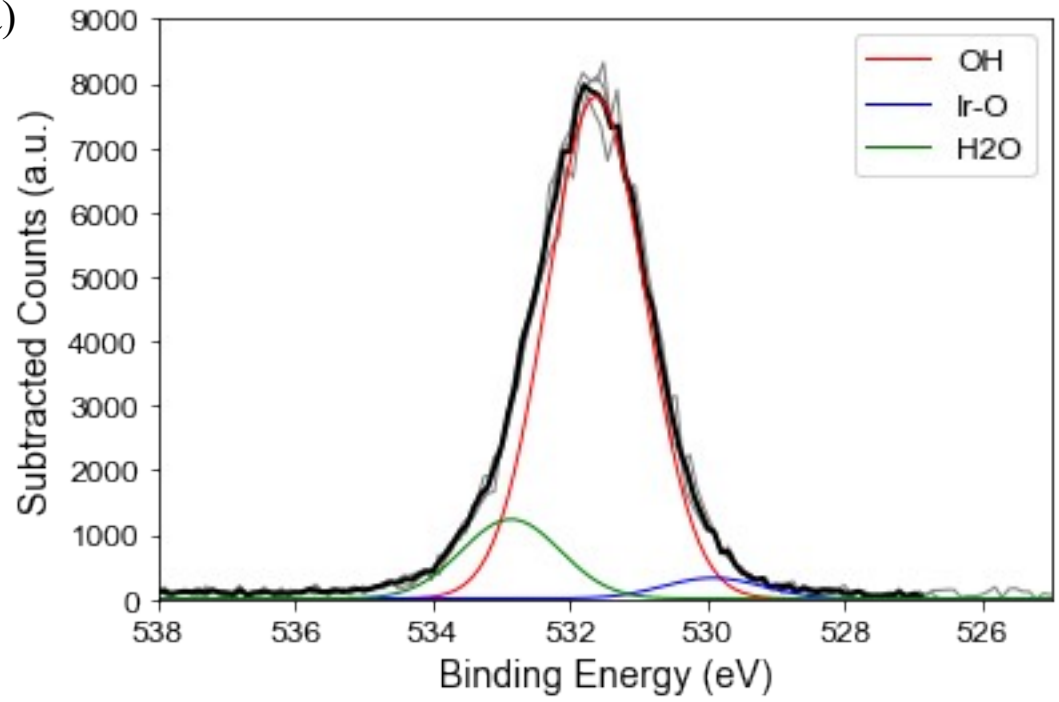

(b)

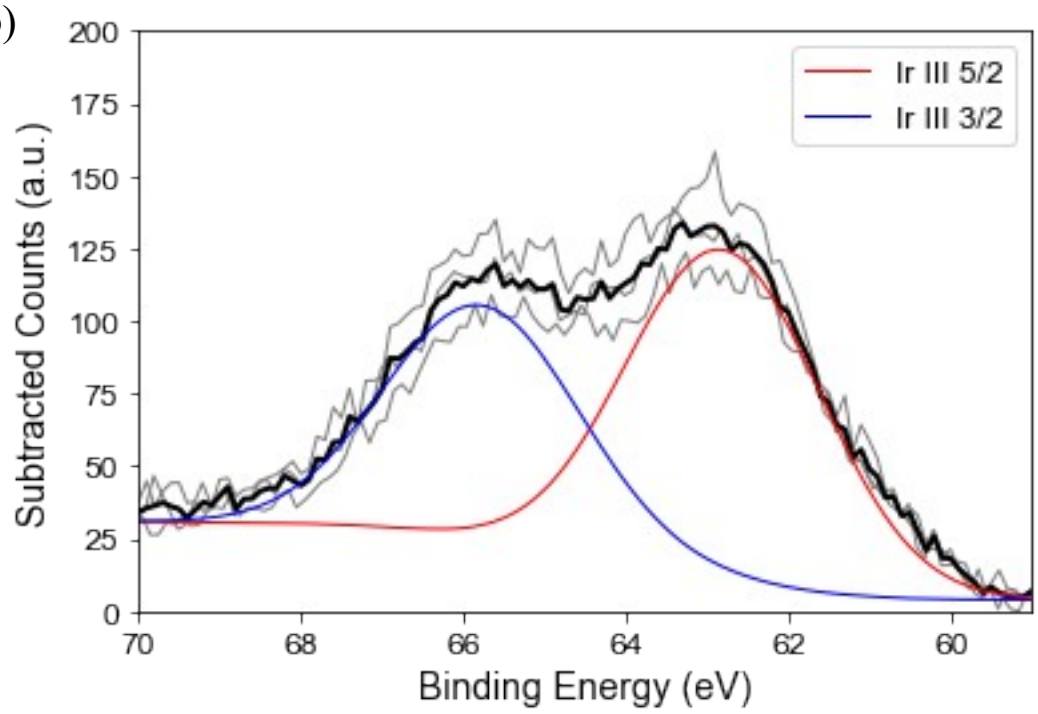

(c)

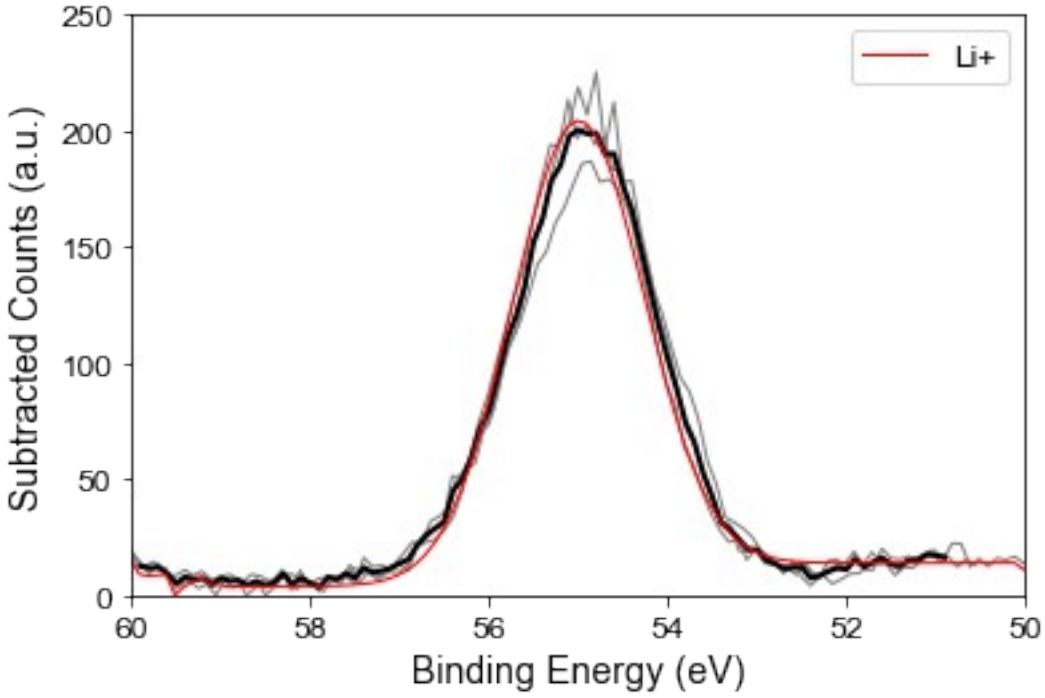
Li+
Subtracted Counts (a.u.)
Binding Energy (eV)
250
200
150
100
50
0
60
58
56
54
52
50

(d)

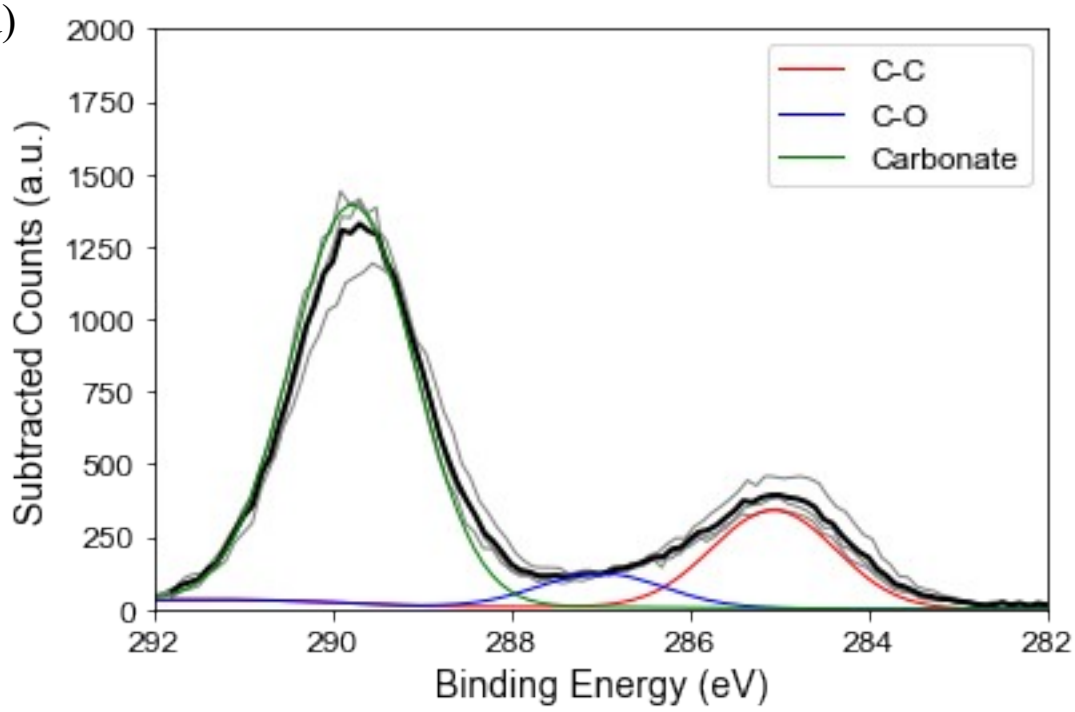
C-C
C-O
Carbonate
Subtracted Counts (a.u.)
Binding Energy (eV)
2000
1750
1500
1250
1000
750
500
250
0
292
290
288
286
284
282

Figure S1. Representative high resolution XPS scans of (a) O 1s electron, (b) Ir 4f, (c) Li 1s, and (d) C 1s drop on Li-IrO_x casted on FTO at 120 ˚C. For each XPS figure, the light grey spectra are raw data for each replicate and the black spectrum is an average of all replicates. Note that the peak fits shown correspond to one of the raw data (grey) spectra deemed similar to the average spectrum. Satellite peaks for iridium (at approximately 63.5 eV and 66.5 eV energy) were not fit as they proved unnecessary for a complete and accurate fit.

S2. Plotted Scan Rate Data for ALD-SnO_2

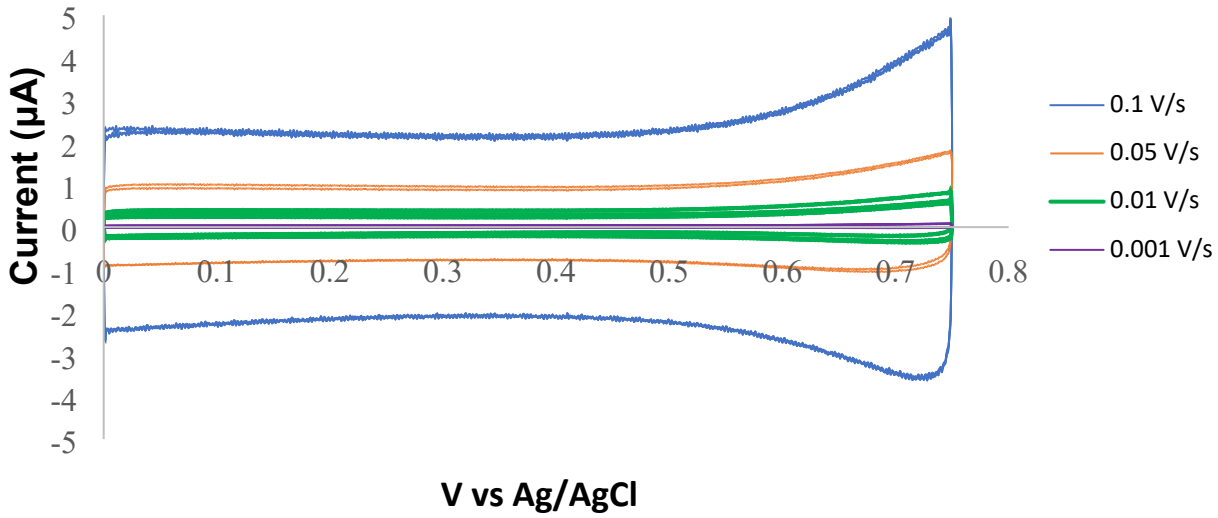

Figure S2. Representative CVs at different scan rates for ALD-SnO_2 AgCl in pH 7, 0.1 M KPi buffer where the blue line is 0.1 V/s, orange is 0.05 V/s, green is 0.01 V/s and purple is 0.001 V/s.

S3. Further Discussion of Deposition of Li-IrO_x

In order to better replicate the previous work using Li-IrO_x, the Li-IrO_x catalyst was sprayed onto the device using a nebulizer.[1] A handheld nebulizer (Hudson RCI, Micro Mist) was used with air to deposit 1.0 mL a 95:5 v/v ethanol: water mixture containing 2.5 mg of Li-IrO_x. The back end of the device covered using parafilm to minimize losses of the deposition solution. The air pressure used was the minimum value sufficient to nebulize the solution. This value was not measured, but the manufacturer reports this value to be 8 liters per minute. As the device aperture was larger than the anode, a short channel was constructed out of parafilm in the shape

and size of the anode in order to ensure all of the solution was deposited onto the anode in the correct area. Additionally, it was thought that this would minimize inconsistency that could occur if manual scanning across the anode with the nebulizer was done. The anode was then heated to 120 °C under air. The precise catalyst loading was not determined.

S4. Open-Circuit Photovoltage Measurements and Recombination Rate Calculations

Under illumination, the quasi-Fermi energy ($E_{F,n}$) of electrons in the nano-SnO_xC_y substrate is determined by the relative rates of injection of both the injection of electrons from the photoexcited PMPDI and the sum of all recombination equations. As such, the modified diode equation (eq S1), where k_B is the Boltzmann constant (eV/K), T is the temperature (K), and e is the elementary charge), at 25 °C, can be used to determine *relative* change in the rate of recombination.[2–4]

$$V_{oc} \propto \frac{k_B T}{e} \ln\left(\frac{\text{rate}_{\text{charge in}}}{\text{rate}_{\text{charge out}}}\right) \quad \text{(S1)}$$

To calculate this change the constant value out front can be calculated as k_B multiplied by temperature divided by e, resulting in 25.85mV. For the anodes studied herein, A (-) shift in V_{oc} occurs due to a (+) shift in $E_{F,n}$ (what we were actually measuring, vs. Ag/AgCl). In the case of a change of -70 mV in the V_{oc} as observed with Li-IrO_x addition, a 15-fold decrease in recombination relative to the rate of injection can be calculated.

S5. Electrochemically-Active Surface Area Correction

In order to compare the electrochemically-active surface area of the planar and 3-dimensional SnO_2 anodes, the double-layer capacitance was determined. Use of that double-layer capacitance assumes that the two types of SnO_2, nano and ALD SnO_2, have the same electrochemical response. A scalar value was determined by measuring the surface area of the planar SnO_2 anodes using photos of the anodes, and then using ImageJ to obtain the surface area, followed by plotting that surface-area value vs the current at +0.4 V vs Ag/AgCl obtained from cyclic voltammetry scans at varying scan rates, Figure 5. Using eq. S2[2], where i_c is current, A is area, C_d is double layer capacitance, and v is scan rate, the slope of this line was determined to be directly proportional to the double-layer capacitance.

$$|i_c| = AC_d v \quad \text{(S2)}$$

The double-layer capacitance determined from the slope can then be divided by the geometric surface area of the planar anodes, giving a scalar value representing the ratio of the electrochemically active surface area / the geometric surface area.

One caveat here is that due to the different thicknesses of the films (especially that of thick nano-SnO_xC_y), diffusion limitations of the H_2Q could be a factor in the relatively lower photocurrent seen in the nano-SnO_xC_y/PMPDI anodes. However, we think this is unlikely for two reasons. First, we do not we do not observe significant current spiking and then significant decay behavior with H_2Q addition over time, which we would expect to see if there issues with H_2Q diffusion in the anode. Second, using different thicknesses of nano- SnO_xC_y for water oxidation results in differing geometric photocurrent densities.[3] One would assume that if diffusion

limitations were present increasing the thickness of the film and amount of dye would not increase the photocurrent as those new surfaces would be inaccessible.

In a second correction method for comparing the anodes made with planar SnO_2 by ALD to the nano-SnO_xC_y anodes made in house, a correction using dye absorbance was made on photocurrent transient plots examining the sacrificial reductant hydroquinone, H_2Q. Given that it is not known if the dye absorbance or the electrochemically-active surface area is a more accurate correction method for the present systems, the data were also corrected using the higher, 1.0:190 value as well of the planar to nanostructured, electrochemically-active surface area, Figure S3.

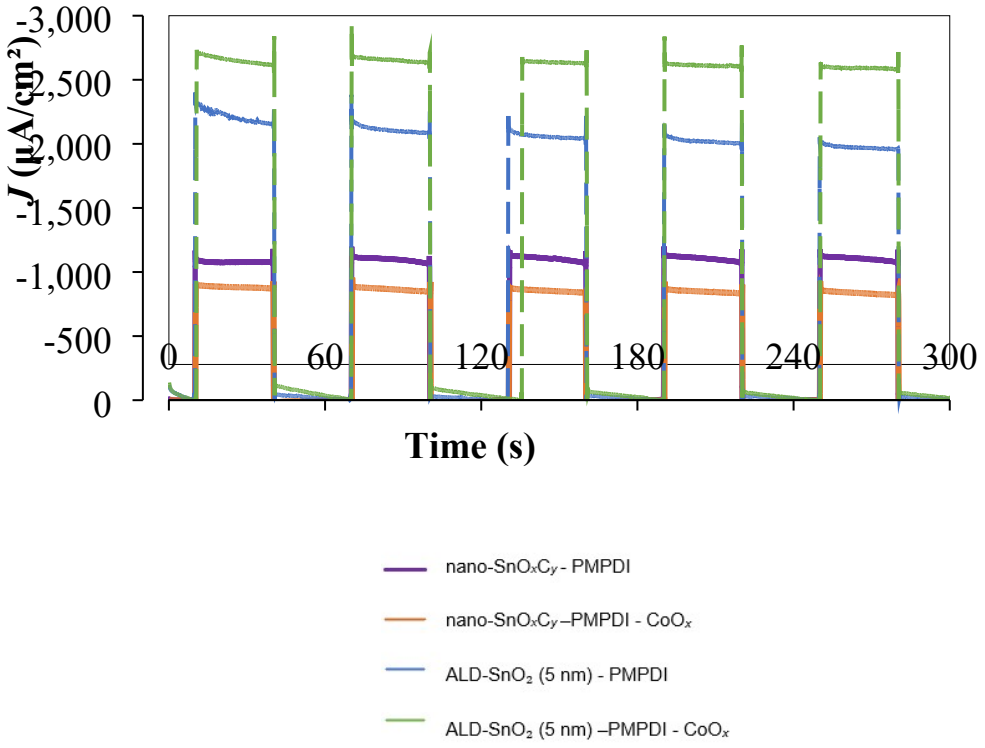

Figure S3. *J*–t transients in the presence of 20 mM H_2Q sacrificial reductant, with background dark current due to dark oxidation of the hydroquinone subtracted, at +0.2 V vs. Ag/AgCl in pH 7, 0.1 M KPi buffer with 30 s light/dark transients where purple is nano-SnO_xC_y/PMPDI, red is nano-SnO_xC_y/PMPDI/CoO_x, blue dashed is ALD-SnO_2(5 nm)/PMPDI (X190), and green dashed is ALD-SnO_2(5 nm)/PMPDI/CoO_x (X190). Both planar (blue and green) anodes are corrected (X190) to match the electrochemically active surface area of the nanostructured anodes.

Given that the corrected data from the planar SnO_2 anodes, using the electrochemically-active surface area as the correction, is significantly higher than the highest values observed in any nanostructured system, it seems likely that the true value for the planar anodes is somewhere between the two limiting, corrected values. Nevertheless, the planar SnO_2 outperforms the nano-SnO_xC_y no matter if the comparison is based on dye absorbance or on the electrochemically-active surface area. The background current does become exaggerated when the planar photoanode's current is scaled up for comparison to the nano-SnO_xC_y anodes, although it should be noted that the resultant, inflated background value is a poor representation of the true background current as well as a poor measure of the anode's photo performance in the dark.

S6. Comparison of our Previously Published Best Performing Anodes with Alumina

In another previous study of ours, we have used ultrathin AlO_n prepared by ALD to improve the water oxidation performance of the SnO_xC_y/PMPDI anode with or without CoO_x WOC.[3] Using the current density correction approach shown here, we can also examine how the choice of ultrathin ALD materials (i.e., AlO_n vs. SnO_2) affects the water oxidation performance. Accordingly, the photocurrent data in buffered water was corrected using the previously determined dye absorbance value in order to be comparable to the nano-SnO_xC_y/PMPDI system and was coplotted with the best performing version of a representative anode, nano-SnO_xC_y/PMPDI/PMPDI/AlO_n (0.6 nm, 85 °C deposition) from the noted previous study[3] that, again, includes an overlayer of AlO_n deposited by ALD, both with and without CoO_x (Figure 7).

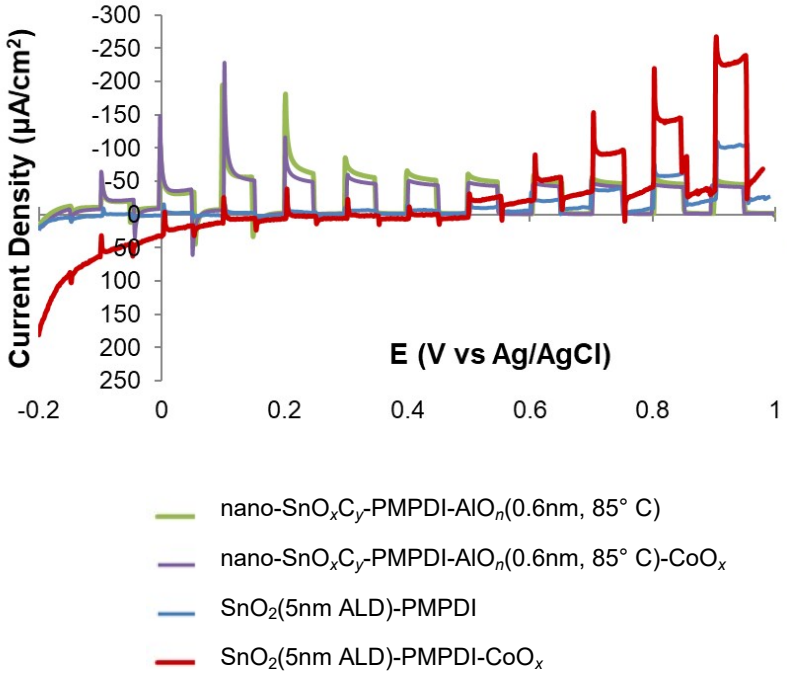

Figure S4. Photocurrent transients for ALD-SnO_2(5nm)/PMPDI (blue, corrected for surface area), ALD-SnO_2(5nm)/PMPDI/CoO_x (red, corrected for surface area), nano-SnO_xC_y/PMPDI/AlO_n (0.6 nm, 85 °C) (green), and nano-SnO_xC_y/PMPDI/AlO_n (0.6 nm, 85 °C)/CoO_x (purple) anodes, all in in pH 7, 0.1 M KPi buffer. Scans were done from -0.2 to +1.0 V vs. Ag/AgCl with 5 s light dark transients.

The anodes made using planar SnO_2 deposited by ALD (red and blue traces; corrected for dye absorbance) were shown to have a higher photocurrent than the previous best nano-SnO_xC_y/PMPDI/AlO_n (0.6 nm, 85 °C deposition)[3] systems (purple and green traces) at potentials over +0.6 V vs. Ag/AgCl.

S7. Photocurrent Measurements on ALD-SnO_2 anodes with and without Li-IrO_x *without* H_2Q

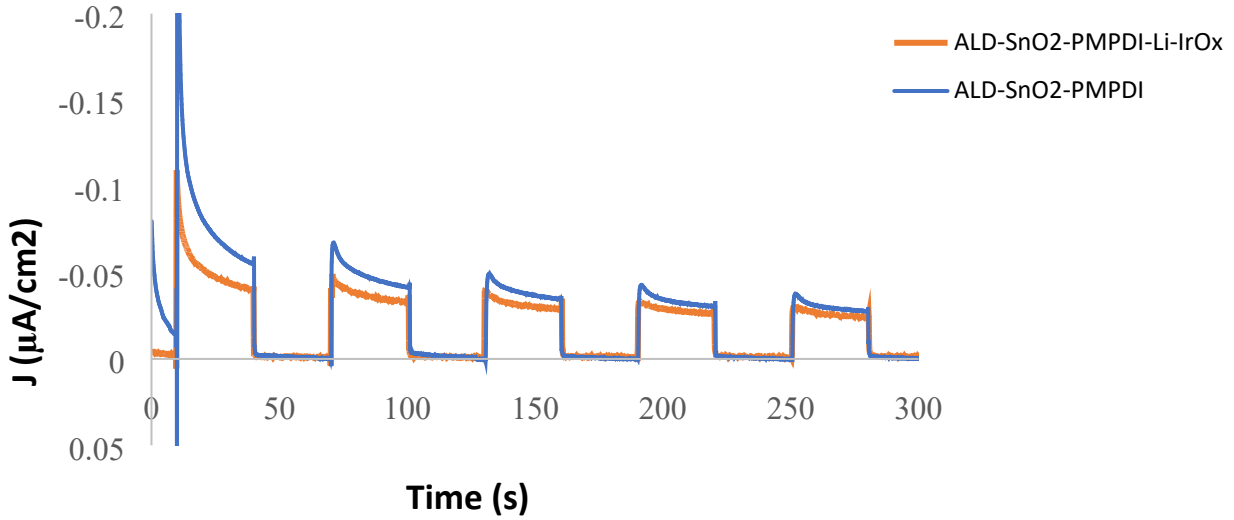

Figure S5: *J-t* transients of ALD-SnO_2/PMPDI with and without Li-IrO_x at +0.2 V vs Ag/AgCl in pH 7, 0.1 M KPi buffer with 30 s light/dark transients where blue is ALD-SnO_2-PMPDI and orange is ALD-SnO_2-PMPDI-Li-IrO_x.

S8. Scheme S1. Proposed, working hypothesis kinetics scheme illustrating the proposed charge-transfer pathways in the nano-SnO_xC_y/PMPDI/Li-IrO_x system

The following scheme, intended as a *working hypothesis for going forward*, is an adaptation of our previous kinetics scheme for the nano-SnO_xC_y/PMPDI/CoO_x system[5].

Scheme S1. Proposed, working hypothesis kinetics scheme illustrating the proposed charge-transfer pathways in the nano-SnO_xC_y/PMPDI/Li-IrO_x system. SnO_2 is white, PMPDI is pink, and Li-IrO_x is purple. Green arrows indicate idealized pathways for charge transfer in water-oxidation catalysis, while red arrows indicate loss of efficiency in the form of charge-carrier recombination. Blue arrows show charge recombination pathways that are attributable to carbon remaining in the nano-SnO_xC_y. For the sake of simplicity all other potential impurities and defects, including O-vacancy defects, are omitted from this scheme.[6] Note here that the catalytic onset of water oxidation by Li-IrO_x on FTO was observed to be 1.2 V vs. Ag/AgCl in pH 7 kPi buffer. One point clear from this scheme is the *kinetics complexity of even our relatively simple WOC device*. It is important to note here that, in comparing the kinetics scheme for the Li-IrO_x and CoO_x catalyst systems, the charge transfer pathways would be depicted identically, other than the location of the catalyst's onset potential, occurring at +1.03 V vs. Ag/Ag/Cl for CoO_x and +1.2 V vs. Ag/Ag/Cl for Li-IrO_x.[3]

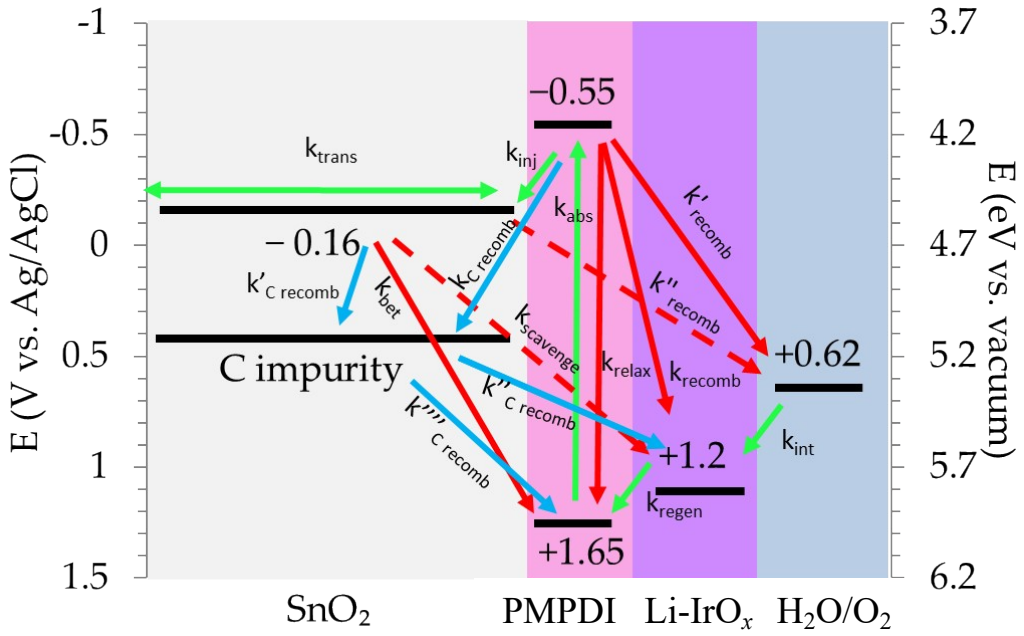

Kinetics pathways for charge transfer are identified in the scheme using k_{trans}, $k_{scavenge}$, k_{inj}, k_{recomb}, k_{abs}, k_{bet}, k_{relax}, and k_{regen} indicating, respectively, electron transfer, scavenging, injection, recombination, absorbance, back electron transfer, relaxation, and regeneration. As mentioned in the figure caption, charge-recombination pathways are shown in red and blue, where blue pathways indicate pathways attributed to carbon defects. Idealized pathways for charge transfer leading to water oxidation catalysis are shown in green. The increased photocurrent and reversal of the "anti-catalyst" effect seen with CoO_x with the use of Li-IrO_x is readily explained by the

hypothesis that recombination originating from pathways attributable to carbon is minimized, while more charge transfer occurs through the optimal green pathways with the more active Li-IrO_x catalyst.

What is not represented in the above kinetic scheme is the changes in the rate constant for each charge transfer pathway that occur by altering the WOCatalyst. Our data are consistent with and fully support the hypothesis that decreased recombination in the systems with Li-IrO_x can be attributed to increased rate constants for charge transfer in pathways involving Li-IrO_x, specifically k_{int} and k_{regen}. These rate constants reflect charge injection from the water oxidation reaction into Li-IrO_x and charge regeneration of the dye from Li-IrO_x, respectively. Finally, we emphasize once more that Scheme S1 is provided only as a working hypothesis for further investigations going forward.

References

(1) Cho, H. H.; Yao, L.; Yum, J. H.; Liu, Y.; Boudoire, F.; Wells, R. A.; Guijarro, N.; Sekar, A.; Sivula, K. A Semiconducting Polymer Bulk Heterojunction Photoanode for Solar Water Oxidation. *Nat Catal* **2021**, *4*, 431–438.

(2) Bard, A. J.; Faulkner, L. R. *Electrochemical Methods Fundamentals and Applications*, 2nd edn.; John Wiley & Sons, Inc.: Hoboken, NJ, 2001.

(3) Kirner, J. T.; Finke, R. G. Sensitization of Nanocrystalline Metal Oxides with a Phosphonate- Functionalized Perylene Diimide for Photoelectrochemical Water Oxidation with a CoO_x Catalyst. *ACS Applied Materials Interfaces* **2017**, *9*, 27625–27637.

(4) Ardo, S.; Meyer, G. J. Photodriven Heterogeneous Charge Transfer with Transition-Metal Compounds Anchored to TiO2 Semiconductor Surfaces. *Chem Soc Rev* **2009**, *38*, 115–164.

(5) Jewell, C. F.; Subramanian, A.; Nam, C.-Y.; Finke, R. G. Ultrathin Alumina Passivation for Improved Photoelectrochemical Water Oxidation Catalysis of Tin Oxide Sensitized by a Phosphonate-Functionalized Perylene Diimide First without, and Then with, CoO_y. *Sustain. Energy Fuels* **2021**, *5*, 5257–5269.

(6) Corby, S.; Francàs, L.; Kafizas, A.; Durrant, J. R. Determining the Role of Oxygen Vacancies in the Photoelectrocatalytic Performance of WO_3 for Water Oxidation. *Chem Sci* **2020**, *11*, 2907–2914.